ACS OMEGA

Open Access

http://pubs.acs.org/journal/acsodf

Article

Optimization of Metal Ion/Fuel Ratio for an Effective Combustion of Monticellite and Investigation of Its Microbial and Hemolytic Activity for Biomedical Applications

Naveensubramaniam Vijayakumar, Senthil Kumar Venkatraman, Ravindiran Nandakumar, Raveena Ann Alex, Jayanthi Abraham, Hossein Mohammadi, Mona Ebadi, and Sasikumar Swamiappan*

Cite This: *ACS Omega* 2023, 8, 36919−36932

Read Online

ACCESS | Metrics & More | Article Recommendations | Supporting Information

ABSTRACT: Bioactive silicates have gained popularity as bone graft substitutes in recent years due to their exceptional ability to bind to host tissues. The current study investigates the effect of changing the metal ion-to-fuel ratio on the properties and biological activity of monticellite prepared via the sol−gel connived combustion technique. Single-phasic monticellite was obtained at 900 °C, without any secondary-phase contaminants for the fuel-lean, stoichiometric, and fuel-rich conditions. SEM and TEM micrographs revealed the porous, spongy morphology of the materials. Because of the reduced crystallite size and higher surface area, the biomineralization of monticellite prepared under fuel-lean conditions resulted in more apatite deposition than those of the other two samples. The results show that the material has a good compressive strength comparable to natural bone, while its brittleness is equivalent to the lower moduli of bone. In terms of antibacterial and antifungal activities, the monticellite bioceramics outperformed the clinical pathogens. It can be used for bone tissue engineering and other biological applications due to its excellent anti-inflammatory and hemolysis inhibitory properties.

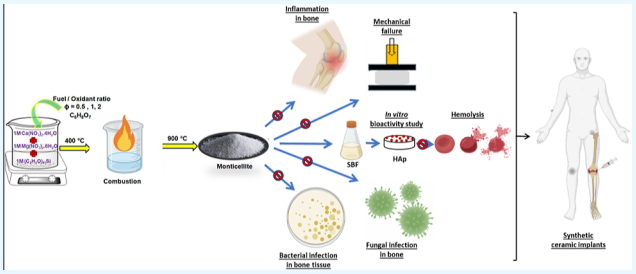

1. INTRODUCTION

Bone is a composite material composed of 70% hydroxyapatite mineral and 30% type I collagen protein, with a dynamic structure of intertwined macro- and micropores.[1−3] Bone flaws and disorders are occuring commonly as a result of traumas, implanting, and postsurgical osteoporosis.[4] In this facet, implants made of bioactive materials have been widely employed as a bone graft alternative to revamp or regenerate damaged tissues rather than the autograft, allograft, and xenograft transplants.[5,6] The ideal biomaterial for implants should be biodegradable, biocompatible, and mechanically strong enough to mimic natural bone while encouraging cell growth.[7,8] Several attempts have been made to engineer or design suitable scaffolds with improved bioactive properties for tissue regeneration.[9] The development of innovative bone scaffolds can make it possible to fabricate suitable constructs to not only regenerate the bone but also deliver therapeutic molecules locally to the site of action. Bone scaffolds are three-dimensional constructions made up of biomaterials that are utilized for the restoration of bone defects.[10] The purpose of a scaffold is to act as a synthetic and temporary duplicate of the extracellular matrix, which facilitates cell attachment and directs the development of a three-dimensional bone tissue.[11]

Bioactive ceramics have piqued the tenacious interest of researchers and are an indispensable component in overcoming the perplexity in bone tissue engineering.[8] Silicate ceramics are now widely used as an effectual bioactive implant owing to their ability to direct bone affixing at the interface of the material and invigorate the biological activity of the implant through the formation of new bone cells.[6,12] Now, far more consideration has been paid to the calcium−magnesium silicates with improved mechanical strength, meticulous resorbable proportion coupled with better in vitro properties.[13,14] The apatite deposition ability of several ternary silicates such as diopside, akermanite, monticellite, and merwinite was doled out and reported to be bioactive by HAp nucleation at different rates.[15−19] Amid them, monticellite with an optimal ratio of Ca, Mg, and Si combination was chosen as a choice for the bone graft substitute, whose material properties and bioactive nature are still unexplored. Only a few reports on the biocompatibility and bioactivity of the material have been published so far. Monticellite was found to be biologically active with similar chemical constituents and mechanical strength equivalent to that of human cortical bone,

Received: June 6, 2023
Accepted: August 16, 2023
Published: September 26, 2023

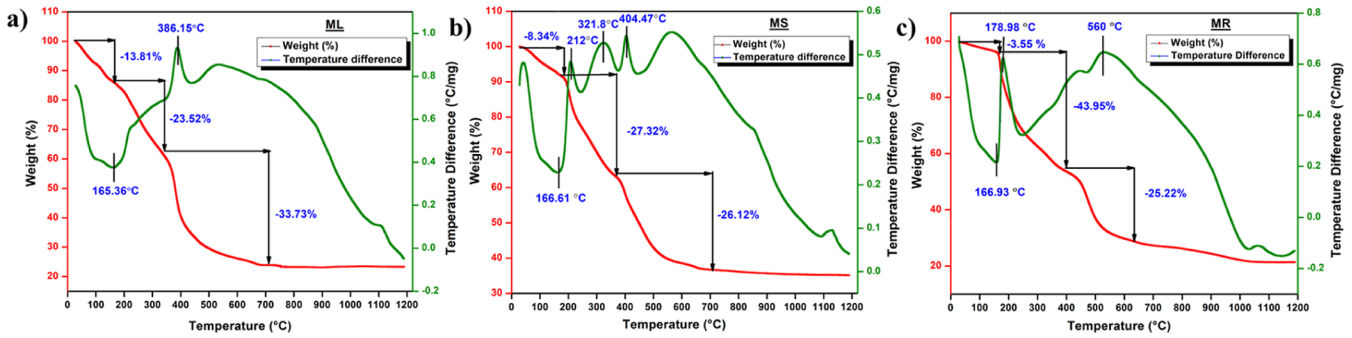

Figure 1. TGA/DTA thermograms of dried gel (a) ML, (b) MS, and (c) MR.

making it a promising material for bone graft replacement for implants and coating materials.[20]

Investigation on the currently available biomaterials including metals and polymers is proven to be ineffective to be employed as bone graft substitutes owing to their lack of biomineralization and inferior load bearing properties.[21] To have better load bearing ability for bone graft substitutes, ceramic biomaterials make a better replacement with the currently available transplant materials. One of the silicate-based ceramics is monticellite with the chemical composition of $CaMgSiO_4$. According to the literature findings, Ma et al. have reported that monticellite bioceramics formed apatite formation on its surface after soaking in SBF solution, which indicates in vitro bioactivity.[22−24] Additionally, Koroglu et al. have shown that the bioactivity and apatite-forming ability of monticellite could be governed by the particle size of monticellite powders, surface feature, and sintering temperatures.[23,25] Besides, monticellite supported the differentiation and proliferation of bone cells.[24,26,27] Furthermore, it has a higher Young's modulus and fracture toughness compared to hydroxyapatite (HAp), which is closer to human cortical bone.[26]

Bioactive materials used in implants must have effective bactericidal activity.[21] Septic arthritis, osteomyelitis, and prosthetic joint infections are the most common human bone disorders that result in bone cell obliteration.[6] Earlier reports stated that implant failure was caused by bacterial contagions that occur during surgeries and impinge on the surrounding tissues of human organs.[28] In this regard, designing a material with improved bactericidal activity is an additional requirement for an implant material to combat bacterial infections.[6,21] Barely, a few reports on the bioactive nature and antibacterial exertion of monticellite are available, and it is still not probed to figure out the requirements for fusing it as a bone graft supplant for neoformation of bone tissues. Bakhsheshi-Rad et al. reported that scaffolds containing monticellite-ciprofloxacin exhibited a remarkable antibacterial action against *Escherichia coli* and *Staphylococcus aureus,* and drug release properties make the material more prominent for bone reinstatement utilization.[29]

A variety of synthetic approaches were used to obtain the desired phase of the material. Synthesis processes are important in the development of an optimal biomaterial as they influence the material's properties.[24] Several methodologies, including solid-state, hydrothermal, coprecipitation, and sol−gel processes, have been used to produce the ceramic material, as per the earlier findings.[27,31,32] The preceding synthesis processes necessitate a high-temperature reaction and are neither energy- nor time-intensive.[6,30] The traditional sol−gel technique with combustion assistance is commonly used to prepare nanocrystalline products at low temperatures.[33]

The selection of appropriate fuel is critical for the combustion process as it ignites the reaction between the reactants at a low temperature by preserving the chemical homogeneity.[34] For the production of nanocrystalline zirconia, Boobalan et al. examined the impact of metal ions on fuel proportion in the fabrication of zirconia by a solution combustion method.[35] The primary goal of this research is to achieve monticellite using the sol−gel combustion technique by optimizing the metal ion-to-fuel ratios in terms of fuel-lean, stoichiometric, and fuel-rich conditions. The ignition temperature and the metal ion-to-fuel ratio are the two most important factors that influence the change in phase formation temperature, particle size, morphology, and chemical homogeneity in the combustion reaction.[36] After being immersed in SBF media, the biomineralization capabilities and mechanical strengths of three different materials were evaluated. In addition, bacterial growth inhibition, antifungal, anti-inflammatory, and antihemolysis properties were also investigated to evaluate it for tissue engineering applications.

2. RESULTS AND DISCUSSION

2.1. Synthesis of Monticellite. Monticellite was synthesized by implementing the sol−gel combustion method which aids phase formation at low temperatures. Citric acid was employed as a fuel as it provides high exothermicity at low ignition temperature.[28] The addition of citric acid in the reaction mixture prevents precipitation of metal ions and acts as a gelling agent. TEOS on addition forms the miscellaneous layer because of its insolubility in water. To accelerate the hydrolysis of TEOS into silanol and ethanol, the pH of the solution was changed to acidic (pH = 1−2) using conc. HNO_3. The metal−citrate complex then undergoes a polycondensation reaction with silanol, resulting in the formation of a gel network with water and ethanol. With the evolution of heat energy, the gel is dried and decomposed at 400 °C. The precursor obtained after combustion is calcined at different temperatures (700 and 900 °C) to attain the authentic phase of the material.

Hydrolysis (acid-catalyzed by HNO_3)

$$Si(OC_2H_5)_4 + 4H_2O \rightarrow Si(OH)_4 + 4C_2H_5OH \quad (1)$$

Monticellite—fuel-lean condition (ML)

https://doi.org/10.1021/acsomega.3c03984
ACS Omega 2023, 8, 36919−36932

$$Ca(NO_3)_2{\cdot}4H_2O + Mg(NO_3)_2{\cdot}6H_2O + Si(OH)_4 + 0.5\,C_6H_8O_7 + 0.5O_2 \xrightarrow{\Delta} CaMgSiO_4 + 3CO_2 + 14H_2O + 2N_2 + \text{Heat} \quad (2)$$

Monticellite—Fuel stoichiometric condition (MS)

$$Ca(NO_3)_2{\cdot}4H_2O + Mg(NO_3)_2{\cdot}6H_2O + Si(OH)_4 + 1.11\,C_6H_8O_7 \xrightarrow{\Delta} CaMgSiO_4 + 6.66CO_2 + 16.44H_2O + 2N_2 + \text{Heat} \quad (3)$$

Monticellite—fuel-rich condition (MR)

$$Ca(NO_3)_2{\cdot}4H_2O + Mg(NO_3)_2{\cdot}6H_2O + Si(OH)_4 + 2C_6H_8O_7 + 9O_2 \xrightarrow{\Delta} CaMgSiO_4 + 12CO_2 + 20H_2O + 2N_2 + \text{Heat} \quad (4)$$

2.2. Characterization of Monticellite. *2.2.1. Thermal Analysis.* The thermal analysis of monticellite precursors prepared using various metal ion−fuel ratios is shown in Figure 1a−c. The thermal study was conducted in an O_2 environment at temperatures ranging from ambient temperature to 1200 °C. In Figure 1a−c, a consistent weight loss of roughly around 4−13% was observed up to 150 °C due to the removal of water molecules from the gel precursors of monticellite. In all the three predecessors, the TGA thermogram of monticellite revealed a weight reduction of roughly 23, 27, and 44%, respectively. The fuel breakdown from the gel matrix might account for the normal weight loss reported in the region of 250−400 °C. From 400 to 800 °C, the removal of carbon and nitrate moieties from the gel matrix of ML, MS, and MR resulted in a considerable weight loss of around 25−35%.[31,37]

In DTA curves, Figure 1a (ML) shows an exothermic peak at 386 °C and an endothermic peak at around 160 °C, which are attributed to the fuel disintegration and the removal of organic wastes and moisture content, respectively. Figure 1b (MS) shows a triplet exothermic peak and a singlet endothermic peak, whereas Figure 1c (MR) exhibits two exothermic and an endothermic peak. The exothermic peaks at around 200−400 °C correlated with the decomposition of fuel and the elimination of organic and nitrate moieties during the redox process. The development of periclase and the elimination of carbonaceous impurities were linked to the exothermic peak at around 410 and 560 °C, respectively. The endothermic peak at 160−170 °C was recognized as the elimination of water moieties.[38,39] Even though the chemical composition of all the three samples remains the same, they show different thermograms due to changes in the metal ion-to-fuel ratio. It is evident from DTA that the decomposition temperature increases for fuel-lean conditions as the exothermic peak is observed at 386 °C, whereas under fuel-rich conditions, the combustion takes place at 179 °C, which is found to be very low and close to the autoignition temperature of citric acid. This argument is well supported by the TGA curve, as there is a huge weight loss close to this exothermic peak, which proves that combustion takes place at this stage. For the stoichiometric ratio of the fuel, the curve shows a 3-fold degradation in this region, which indicates that the pathway for combustion is different. From the obtained results, it is well proved that the fuel−oxidant ratio decides the thermochemistry of the reaction, which influences the different phase formation at the end of the process.

2.2.2. Functional Group Identification. Figure 2 represents the Fourier transform infrared (FT-IR) spectra of monticellite

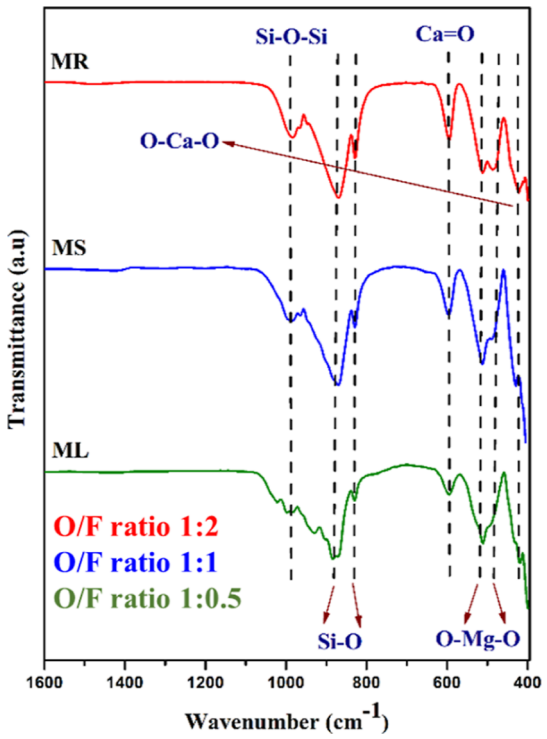

Figure 2. FT-IR spectra of monticellite for ML, MS, and MR.

with different oxidant-to-fuel ratios calcined at a temperature of 900 °C for 6 h. The analysis of the presence of functional group helps us to know the transformation of the material into its final product from the starting materials. From Figure 2, it can be observed that monticellite showed bands at 870 and 830 cm^{-1} corresponding to SiO_4 tetrahedron vibrations. In addition, with that, the peaks spotted at 511 and 487 cm^{-1} are assigned to the O−Mg−O bending vibrational modes. The Si−O−Si functional group exhibited a symmetrical stretch out which is witnessed with a peak appearing at 984 cm^{-1}. The frequency band comes into sight at 424 cm^{-1}, recognizing the O−Ca−O vibrations. The spectral bands obtained for monticellite at 900 °C clearly indicate the formation of the desired product with all the functional groups, which are in reliable accordance with the previous findings.[13,15,40]

2.2.3. Phase Evolution Studies. Figure 3 shows the X-ray diffraction (XRD) patterns of monticellite under fuel-lean (ML), stoichiometric (MS), and fuel-rich (MR) conditions at different steps of calcination. High intense peaks of monticellite with complete elimination of impurities were observed at 900 °C (Figure 3a), resulting in the development of a single-phasic monticellite, which was matched and indexed with a standard JCPDS data card (96-900-1078).

Figure 3 depicts the monticellite's phase evolution patterns. According to the findings, the gel decomposes at around 170−400 °C depending on the fuel ratio, revealing the development of the calcite as the major phase. Even after 6 h of calcination at 700 °C, periclase (MgO) and merwinite were detected. Thermal treatment at 900 °C for 6 h resulted in the removal of secondary-phase impurities and achieved single-phasic mon-

https://doi.org/10.1021/acsomega.3c03984
ACS Omega 2023, 8, 36919−36932

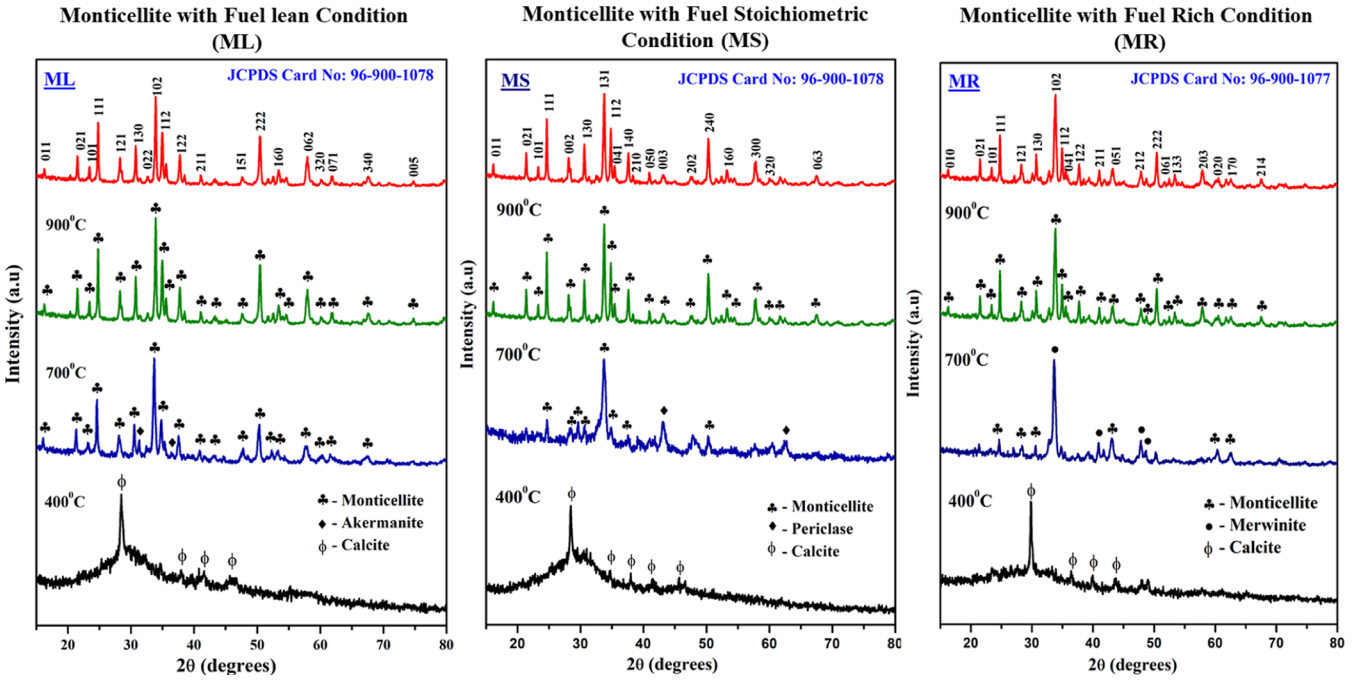

Figure 3. XRD patterns of monticellite with different fuel conditions.

ticellite. Monticellite's XRD patterns were fitted and indexed with respect to the standard JCPDS data card: 96-900-1078 and 96-900-1077. Earlier investigations unveiled that monticellite was generated following calcination at temperatures between 1200 and 1400 °C. According to the reports about concocting monticellite, Chen et al. got the monticellite phase at 1480 °C by using the sol−gel sintering method. At a temperature of 1300 °C, Koppala et al. reported in a recent research that the akermanite phase occurs alongside the monticellite phase during the synthesis of monticellite utilizing a variety of fuels.[17,20,30] Astoundingly, the pure phase of monticellite was procured without secondary-phase impurities by utilizing the sol−gel combustion technique at a calcination temperature of 900 °C. Monticellite for the above conditions was found to own an orthorhombic crystal system. The results are well in agreement with the findings from thermal analysis, as the precursors calcined at 400 °C show different phases for different conditions, but further heat treatment results in a pure product for all the three conditions. The crystallite size was determined using the Debye−Scherer equation (eq 5). The lattice parameters and crystallite size of monticellite powders are shown in Table 1.

$$D = \frac{0.89\lambda}{\beta \cos\theta} \tag{5}$$

2.2.4. Microstructural Analysis. The SEM and TEM micrographs of the synthesized bioceramics after calcination at 900 °C are exposed in Figure 4a−f, respectively. The surface morphology of the monticellite powders shows agglomerated, dense, and irregular particles, as shown in the micrographs. In addition, all the three samples possess spongy morphology with pores distributed across the surface of the materials. The porous nature of the materials appeared due to the elimination of gaseous products during the decomposition of fuel. It was observed that the pores obtained are found to be nanopores. The anticipated porosity of the scaffold consists of macropores, on purpose designed to facilitate bone cell proliferation, with a minimum size exceeding 100 μm.[41] The aggregation of particles caused the grain size to grow, which was evident from the TEM micrographs. The selected area electron diffraction pattern validated the produced material's high crystallinity. The SEM micrographs agree with the results obtained through thermal analysis and powder XRD analysis, as the particle size and agglomeration are found to be increasing with an increase in fuel quantity.

Table 1. Lattice Parameters and Crystal Size of Monticellite Bioceramics

	cell parameters (Å)			
sample code	*A*	*B*	*C*	crystalline size (nm)
ML	4.8042	11.0320	6.3458	27−31
MS	4.7993	11.0261	6.3363	29−33
MR	4.8272	11.0776	6.3739	31−34

2.3. In Vitro Biomineralization of Monticellite. After implantation, bone graft substitutes should not only possess adequate mechanical strength but also exhibit an appropriate interaction with the surrounding host tissues. One of the primary prerequisites for a bone graft replacement is its ability to facilitate the deposition of apatite at the interface between the implant and the patient's bone. When exposed to a physiological environment, the implant material develops an apatite layer on its surface, which may be used to evaluate the material's biomineralization capacity.[42]

The comparative research of monticellite's HAp nucleation capacity achieved under various fuel ratio circumstances is shown in Figure 5a−c. The prepared monticellite pellets submerged in a physiological medium were replaced every 24 h to ensure a steady supply of ions required for effective biomineralization. The growth of an apatite layer on the submerged pellets can be seen in ML, MS, and MR following the third day of immersion, as shown in the above image. Based on the findings, the development of the HAp layer on

https://doi.org/10.1021/acsomega.3c03984
ACS Omega 2023, 8, 36919−36932

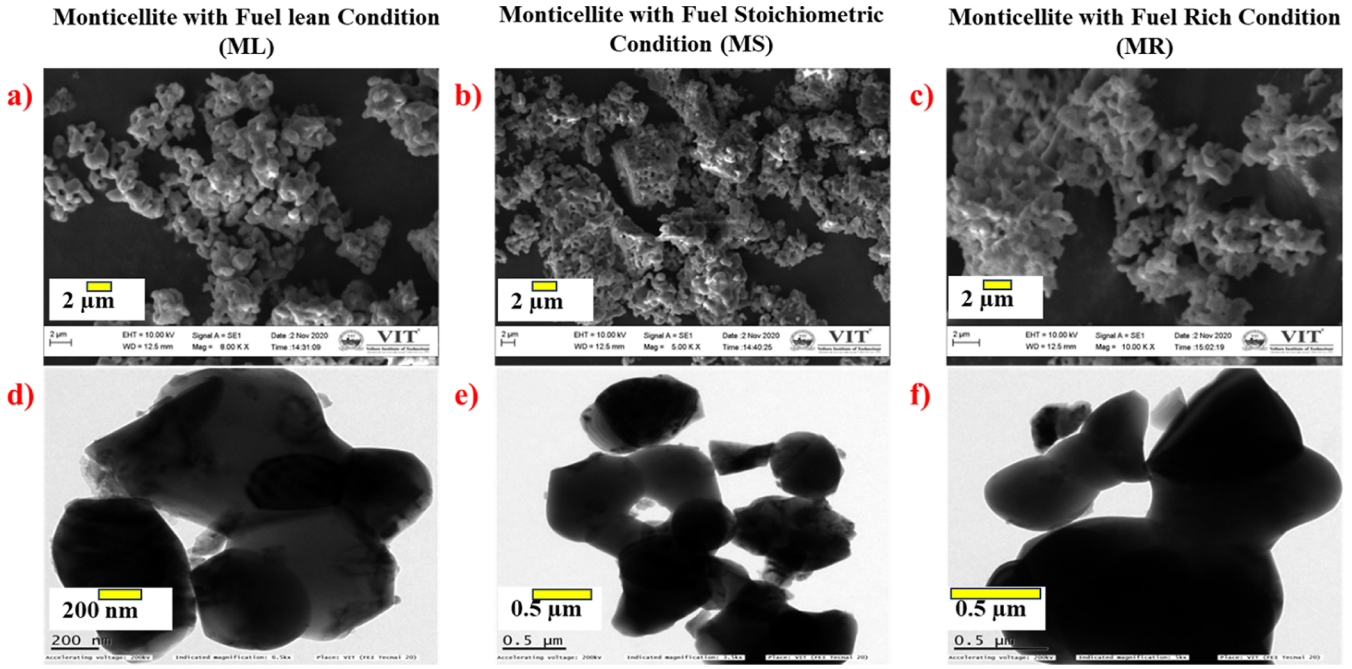

Figure 4. SEM and TEM micrographs of (a,d) ML, (b,e) MS, and (c,f) MR. The scale bar = 2 μm for images (a−c), 0.5 μm for images (e,f), and 200 nm (d).

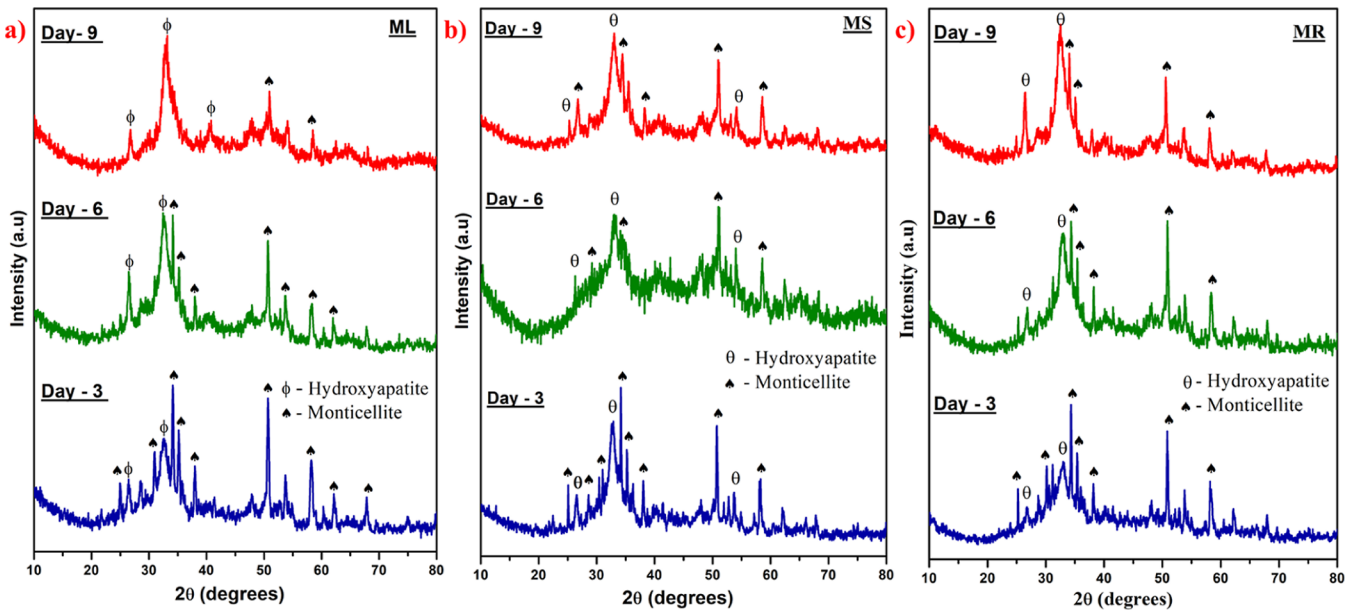

Figure 5. XRD patterns of monticellite immersed in SBF (a) ML, (b) MS, and (c) MR.

the surface of the monticellite pellets has started after 3 days of immersion in SBF. As mentioned earlier, the presence of the optimum ratio of silica content (38.4%) in monticellite instigates the deposition of the hydroxyapatite layer on the pellets.[43] Though apatite peaks were observed to be intense on the sixth day, the appearance of monticellite peaks was noticed and remains unchanged, which indicates that the monticellite surface is not completely covered with a hydroxyapatite layer.

After the ninth day of immersion, the XRD patterns of monticellite produced in a fuel-starved (ML) environment revealed amorphous apatite covering the major surface of the pellet, whereas the XRD patterns of stoichiometric and fuel-rich condition-derived monticellite scaffolds showed partial accretion of apatite on the scaffold's surface. The XRD patterns of HAp were compared and matched with those of the JCPDS card (09-0432). According to a previous research, monticellite exhibited apatite nucleation after 2 weeks of immersion in the SBF medium. High phase formation temperature, which results in an increase in the crystallite size and secondary-phase impurities associated with the material, suppresses the rate of apatite deposition. Koppala et al.'s investigation on the bioactivity of monticellite revealed that the apatite nucleation was initiated only after the 10th day of immersion in the physiological medium, whereas the composites of monticellite with HAp prepared by Kalantari et al. showed the apatite formation on 14th day after being immersed in the body fluid

https://doi.org/10.1021/acsomega.3c03984
ACS Omega 2023, 8, 36919−36932

medium.[30,43,44] Furthermore, ML, MS, and MR exhibited an increased intensity of the apatite peaks on the sixth day compared to that on the third day of submersion. From the above observations, it was found that fuel-lean condition-derived monticellite exhibited a higher biomineralization ability compared to the other two samples. The reason behind the greater bioactivity was due to the smaller particles which provide greater surface area and hence show more apatite deposition, which leads to the complete coverage of the surface, whereas the stoichiometric and fuel-rich condition sample with higher particle size ends up in moderate surface coverage by the hydroxyapatite layer at the end of the bioactivity studies. The foregoing findings revealed that fuel conditions had a significant impact on particle size and surface area, which affect the material's biological reaction to human cell tissues.

The FT-IR spectra of monticellite with different fuel conditions after the bioactivity are represented in Figure 6.

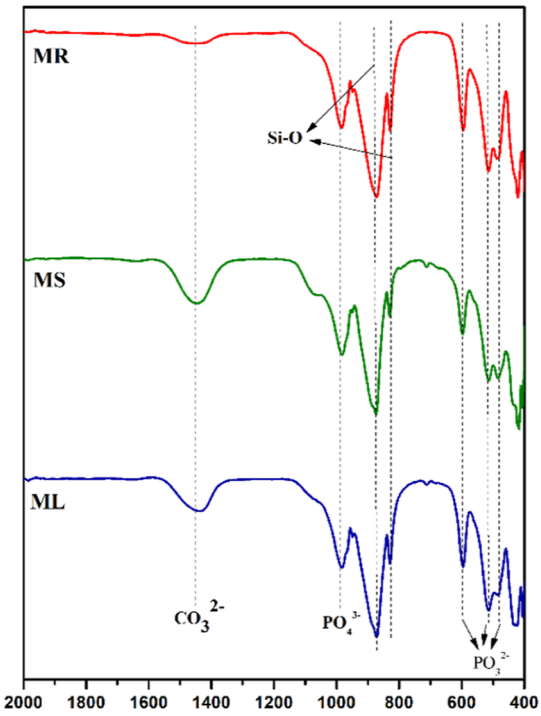

Figure 6. FT-IR spectra of monticellite after bioactivity for ML, MS, and MR.

The peaks appeared in the range 1400−1500 cm^{-1} correspond to the presence of the CO_3^{2-} vibrational modes. In addition to that, the presence of vibrational bands at 1000−1100 and 470−600 cm^{-1} indicates the appearance of stretching and bending frequencies of phosphate groups in ML, MS, and MR, respectively. The absence of absorption bands of metal oxides was due to the dissolution of metal oxides on soaking the pellets in the SBF medium during the process of biomineralization. The formation of the CO_3^{2-} and PO_4^{3-} bands indicates the presence of carbonated apatite deposition over the surface of the immersed pellets. The frequency bands were found to be in accordance with the previous findings.[20,37]

The SEM micrographs and EDX spectra of monticellite scaffolds (a-ML, b-MS, and c-MR) following immersion in SBF media are shown in Figure 7. The appearance of spherical beads on the surface from SEM micrographs revealed the formation of apatite after 9 days of soaking. The elemental composition was scrutinized, and the EDX spectrum pointed out the existence of Ca and P ions with other essential ions validating the deposition of Ca−P on submersion in the physiological conditions. EDX results agree with powder XRD analysis after bioactivity as phosphate quantity is higher under fuel-lean conditions, whereas it is found to be less for fuel-rich conditions. It might be due to the increase in the crystallite size, resulting in a decrease in the surface area for reactivity because of the change in metal ion-to-fuel ratio. The calculated Ca−P ratio of the monticellite scaffolds was found to be in the range of 2.65−3.46 from fuel-lean to fuel-rich conditions, which is closer to the ratio of HAp (1.67). The excessive Ca−P ratio was obtained as the surface of the scaffolds was not entirely covered with the HAp layer, and this may be attained by increasing the soaking time of the scaffolds in the body fluid medium.

2.4. Mechanical Studies. Engineering or designing a bone graft substitute for replacement of the diseased tissues is the ultimate goal in the field of tissue regeneration. In order to provide the necessary structural support, these materials must be able to withstand the mechanical stresses they would encounter when implanted at the location of the defect; their mechanical qualities should resemble those of the human tissues they are intended to replace. The mechanical strength of monticellite scaffolds was analyzed using UTM-INSTRON 8801 after immersion in the physiological medium.[45]

Figure 8a,b depicts the compressive strength and Young's modulus of monticellite at various fuel conditions. The mechanical stability of the material is an essential factor in deciding the load-bearing ability for coalescing it as a bone graft substitute. According to a prior study as compared to akermanite and merwinite, with a high MgO concentration, monticellite is found to have greater mechanical stability.[20] When all of the materials were treated to the same sintering temperatures, monticellite with a high fuel concentration exhibited a greater compressive strength in this investigation. Results revealed that fuel-rich condition-derived monticellite was found to possess 1.5 and 4.5 times increased compressive strength when compared to MS (80 MPa) and ML (49 MPa), respectively. The reason for exhibiting higher mechanical stability merely depends on the grain size, and the distribution of pores with the adjacent particles has an effectual influence in deciding the mechanical strength of the material.[46] On the other hand, ML, MS, and MR have Young's moduli of 1.23, 2.04, and 2.27 GPa, respectively. All the three monticellite scaffolds were found to exhibit lower moduli, which might be because of the high brittleness associated with ceramic biomaterials. Moreover, monticellite's compressive strength results were found to be better in comparison with the previous investigation on the mechanical stability of the material which was found to be around 30−40 MPa, respectively.[20,47] However, Young's modulus of the material was found to be lower than the natural cortical and cancellous bone of the human.[48] The mechanical strength results have been given in Table 2.

2.5. Antibacterial and Antifungal Activities. Infections at the site of implantation are a significant concern, as they can lead to implant failure and other complications. Bacteria can colonize the implant surface and form biofilms, which are challenging to treat with conventional antibiotics. Antibacterial studies aim to determine the material's susceptibility to bacterial colonization and the ability to inhibit bacterial

https://doi.org/10.1021/acsomega.3c03984
ACS Omega 2023, 8, 36919−36932

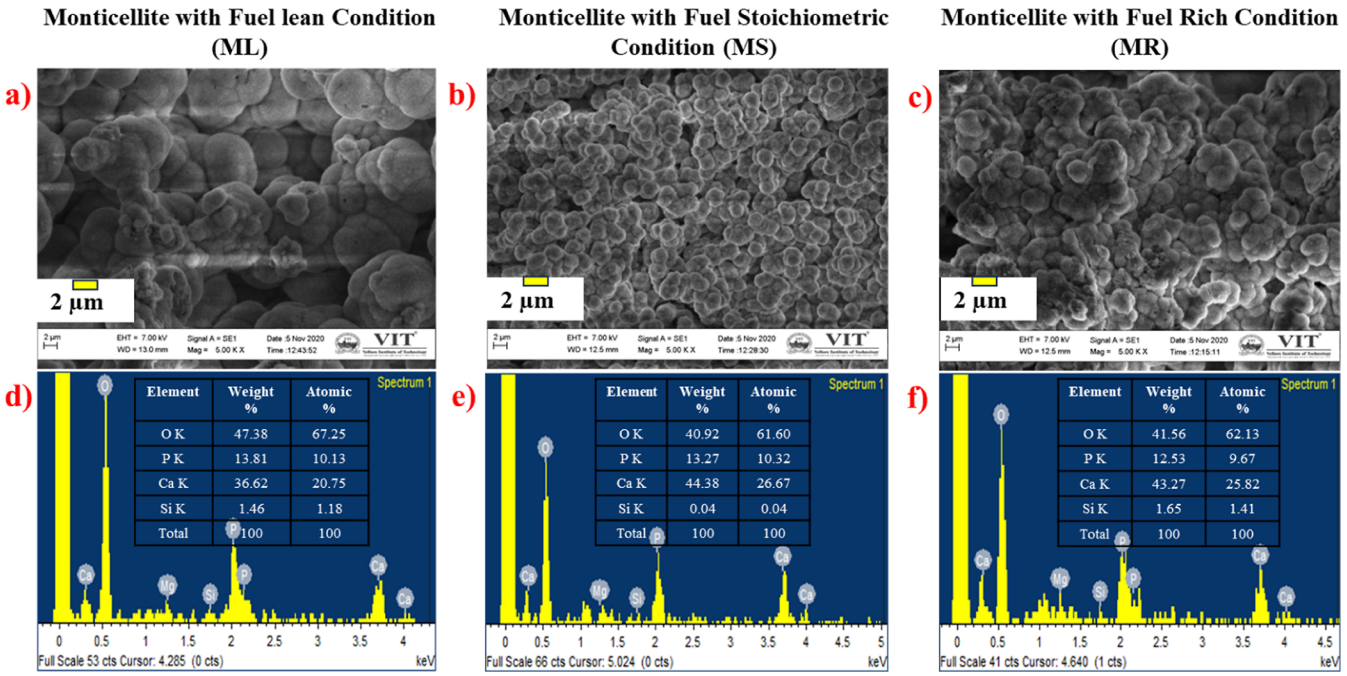

Figure 7. Biomineralization of monticellite after immersion in SBF solution: (a−c) SEM micrographs and (d−f) EDX spectra for ML, MS, and MR. The scale bar = 2 μm for images (a−c).

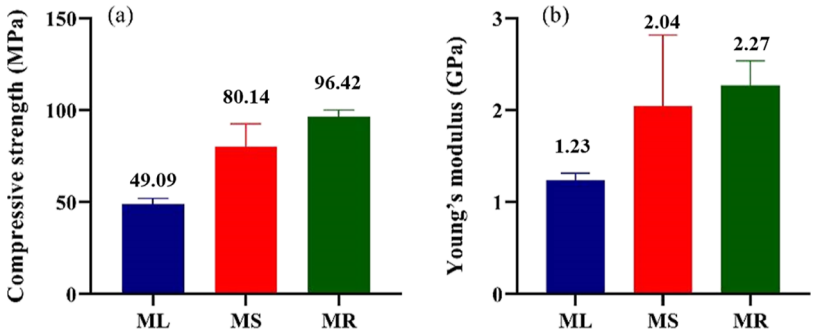

Figure 8. (a) Compressive strength and (b) Young's modulus of monticellite for ML, MS, and MR.

Table 2. Mechanical Strength Values of Monticellite for Different Fuel Conditions

		mechanical properties	
s. no.	sample code	compressive strength (MPa)	Young's modulus (GPa)
1	ML	49.09 ± 1.70	1.23 ± 0.07
2	MS	80.14 ± 4.38	2.04 ± 0.44
3	MR	96.42 ± 3.70	2.27 ± 0.26

growth and biofilm formation. Silicate ceramics with inherent antibacterial properties can reduce the risk of infection and improve the long-term success of the implant.[49]

The antibacterial activity of monticellite ceramic powders ML, MS, and MR was determined using a broth dilution experiment against *E. coli*, *Pseudomonas aeruginosa*, *Staphylococcus epidermidis*, and *S. aureus*. As shown in Figure 9, the experiment demonstrated a greater rate of inhibition against *S. epidermidis* and *S. aureus* (Gram-positive bacteria) than against *E. coli* and *P. aeruginosa* (Gram-negative bacteria). When the findings were compared, *S. epidermidis* exhibited a considerable reduction in growth with an inhibition rate of 83.34 ± 0.1% in ML, 82.60 ± 0.1% in MS, and 85.32 ± 0.1% in MR of monticellite ceramic powders at 2 mg/mL concentration. The culture density was determined by using an ELISA reader. The suspension was composed of monticellite ceramic powder and bacterial strains in Luria−Bertani broth, and the observed results are depicted graphically in Table 3. The antibacterial activity was determined by exposing monticellite ceramic powders to increasing concentrations of 0.5, 1, and 2 mg/mL. At a concentration of 2 mg/mL, the ceramic powder MR inhibited *P. aeruginosa* (Gram-negative bacteria) and *S. epidermidis* and *S. aureus* (Gram-positive bacteria, respectively) more effectively than ML and MS. *E. coli* was inhibited at a lower rate than the other three bacterial strains in all the three monticellite ceramic powder conditions (ML, MS, and MR), whereas *S. aureus* and *S. epidermidis* were inhibited at a greater rate.

Following the broth assay, the antimicrobial activity was determined using the well diffusion method, and the Petri dish images are provided in the Supporting Information (Figures S1 and S2). The selected four pathogenic cultures were swabbed onto Mueller Hinton agar (10^8 cfu/mL), and wells were bored onto the media to which 0.5 1, and 2 mg/mL concentrations of the ceramic powders were added onto the well. The antibacterial activity of monticellite ceramics showed a better

https://doi.org/10.1021/acsomega.3c03984
ACS Omega 2023, 8, 36919−36932

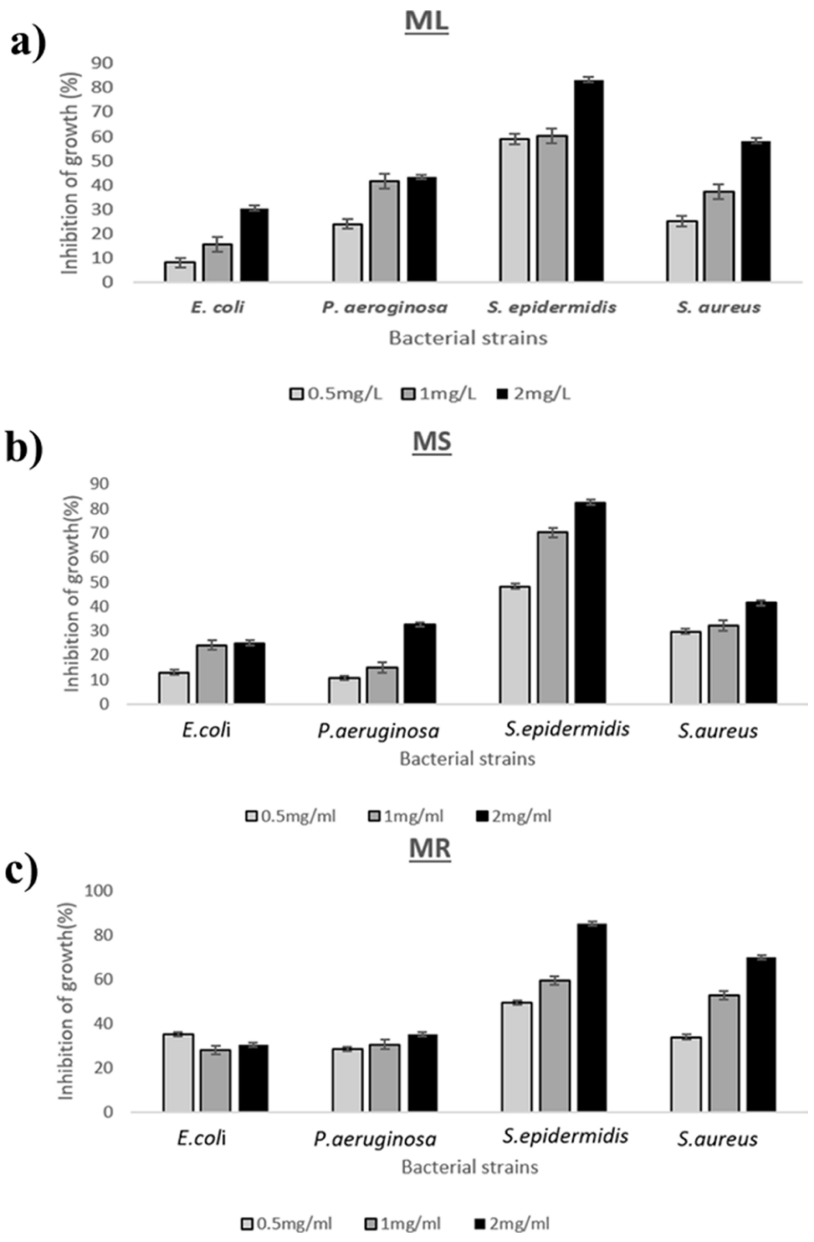

Figure 9. Comparative percentage inhibition of monticellite derived from different fuel conditions: (a) ML, (b) MS, and (c) MR.

Table 3. Percentage of Inhibition of Different Monticellite Ceramic Powders, ML, MS, and MR, against Clinical Pathogens

sample	E. coli (%)	P. aeruginosa (%)	S. epidermidis (%)	S. aureus (%)
ML (0.5 mg/mL)	8.29 ± 0.2	24.05 ± 0.1	58.93 ± 0.1	25.23 ± 0.2
ML (1 mg/mL)	15.81 ± 0.1	41.57 ± 0.1	60.45 ± 0.1	37.34 ± 0.1
ML (2 mg/mL)	30.57 ± 0.1	43.35 ± 0.2	83.34 ± 0.1	58.22 ± 0.1
MS (0.5 mg/mL)	13.01 ± 0.1	10.74 ± 0.1	48.23 ± 0.1	29.76 ± 0.1
MS (1 mg/mL)	24.09 ± 0.1	14.96 ± 0.1	70.21 ± 0.2	32.22 ± 0.1
MS (2 mg/mL)	25.03 ± 0.2	32.57 ± 0.1	82.60 ± 0.1	41.42 ± 0.1
MR (0.5 mg/mL)	35.21 ± 0.1	28.43 ± 0.1	49.60 ± 0.1	34.01 ± 0.1
MR (1 mg/mL)	28.06 ± 0.1	30.63 ± 0.2	59.45 ± 0.1	53.04 ± 0.3
MR (2 mg/mL)	30.41 ± 0.1	35.08 ± 0.1	85.32 ± 0.1	70.01 ± 0.1

inhibition rate against *S. epidermidis* than *E. coli* because of the dichotomy of cellular wall components between *S. epidermidis* as a Gram-positive bacterium and *E. coli* as a Gram-negative bacterium.[29,50] Similarly, from prior reports, it was observed that the *S. epidermidis* strain could be more susceptible than *S. aureus* to the antibacterial and antibiofilm activities of monticellite powders.[44] Table 3 shows the percentage of monticellite ceramic powder inhibition rate by clinical pathogens.

Table 4 depicts the broth's pH variation. After 24 h of incubation, the pH levels increased from 6.8 ± 0.1 to 7.4 ± 0.1, which has a substantial impact on the metabolism of bacteria.

https://doi.org/10.1021/acsomega.3c03984
ACS Omega 2023, 8, 36919−36932

Table 4. Post 24 h Incubation pH Difference of ML, MS, and MR with the Clinical Pathogens

sample	P. aeruginosa	S. epidermidis
control	6.8 ± 0.1	6.8 ± 0.1
ML (0.5 mg/mL)	7.0 ± 0.1	7.1 ± 0.1
ML (1 mg/mL)	7.1 ± 0.1	7.2 ± 0.1
ML (2 mg/mL)	7.4 ± 0.1	7.4 ± 0.1
MS (0.5 mg/mL)	7.1 ± 0.1	7.0 ± 0.1
MS (1 mg/mL)	7.2 ± 0.1	7.1 ± 0.1
MS (2 mg/mL)	7.5 ± 0.1	7.4 ± 0.1
MR (0.5 mg/mL)	7.0 ± 0.1	7.0 ± 0.1
MR (1 mg/mL)	7.1 ± 0.1	7.2 ± 0.1
MR (2 mg/mL)	7.4 ± 0.1	7.4 ± 0.1

The proteins and other cytoplasmic components of the cell are denatured due to high pH, thereby resulting in precipitation in the medium of those materials. Death of bacteria occurs via the rupturing of the cytoplasmic membrane and release of the DNA material. The dissolution of Ca^{2+} and Mg^{2+} ions from monticellite ceramic particles results in a change in pH.[43] After 24 h of incubation, the zone of inhibition was analyzed, and the results recorded are provided in Table 5. It was found that

Table 5. Antibacterial Activity—Zone of Inhibition (in mm) of Monticellite Ceramic Powders against *P. aeruginosa* and *S. epidermidis*

s. no	organism	monticellite ceramic powders (2 mg/mL)	diameter of zone of inhibition of the test samples (mm)
1.	P. aeruginosa	ML	9 ± 0.1
2.	P. aeruginosa	MS	8 ± 0.1
3.	P. aeruginosa	MR	10 ± 0.1
4.	S. epidermidis	ML	13 ± 0.1
5.	S. epidermidis	MS	12 ± 0.1
6.	S. epidermidis	MR	14 ± 0.1

calcium silicate ceramics had a 0.5 mm zone of inhibition after 48 h of exposure to bacteria. *S. epidermidis* was shown to be inhibited by monticellite ceramic powders at a zone of inhibition of 14 mm in the current investigation. The monticellite ceramic powder containing Ca, Mg, and Si ions has the ability to advance antibacterial properties. When compared the results of bactericidal activity of monticellite with earlier findings, it was noted that monticellite when combined with ciprofloxacin was found to have better bacterial inhibition with lower concentrations of ciprofloxacin than pure monticellite against the clinical pathogens.[23] Also, Venkatraman et al. reported that monticellite obtained from eggshell waste was found to exhibit better inhibition against *P. aeruginosa* at a lower concentration of 2 mg/mL due to the presence of magnesium (Mg) content in the structure (Table 5).[24]

The antifungal activity of monticellite powders was tested against two common fungal pathogens, *Aspergillus niger* and *Fusarium oxysporum*. Following the results in Table 6 and from Figures 10 and 11, it was discovered that fuel-lean- and fuel-rich-derived monticellite ceramic powders exhibited more suppression of *F. oxysporum*, whereas stoichiometric condition ceramic powders showed greater inhibition of *A. niger*. When it comes to biomedical application, an ideal biomaterial should

Table 6. Dry Weight of Different Monticellite Ceramic Powders ML, MS, and MR against Clinical Pathogens

sample	F. oxysporum	A. niger
ML (0.5 mg/mL)	0.065 ± 0.1	0.17 ± 0.01
ML (1 mg/mL)	0.063 ± 0.1	0.067 ± 0.01
ML (2 mg/mL)	0.084 ± 0.1	0.062 ± 0.01
MS (0.5 mg/mL)	0.183 ± 0.1	0.152 ± 0.01
MS (1 mg/mL)	0.078 ± 0.1	0.041 ± 0.01
MS (2 mg/mL)	0.059 ± 0.1	0.001 ± 0.01
MR (0.5 mg/mL)	0.074 ± 0.1	0.172 ± 0.01
MR (1 mg/mL)	0.043 ± 0.1	0.074 ± 0.01
MR (2 mg/mL)	0.046 ± 0.1	0.075 ± 0.01

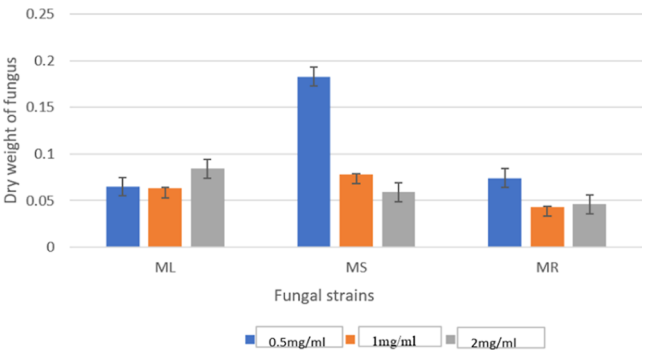

Figure 10. Dry weight of monticellite ceramic powders ML, MS, and MR against *F, oxysporum*.

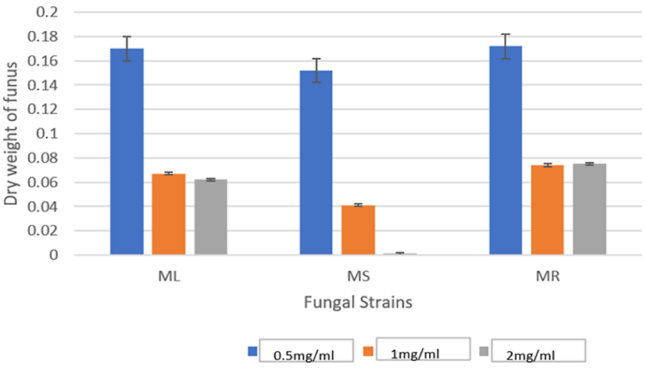

Figure 11. Dry weight of monticellite ceramic powders ML, MS, and MR against *A. niger*.

possess the properties of being both bactericidal and fungicidal as well as being biocompatible with the host tissue or cells when the materials come into contact with them or are on their surfaces. One of the primary reasons why a biomaterial should have these two opposing qualities, namely, one that kills invading microorganisms and the other that maintains cell connection, is due to the fact that bacteria and human cells have a distinct understanding of cell structure. The cell walls of bacteria are made of phospholipids having a negative charge, such as phosphatidylglycerol, phosphatidylserine, and cardiolipin, which are found in abundance. These, in combination with other surface characteristics, impart a negative charge to the cells, which electrostatically attracts cationic antimicrobial chemicals into the cells' interior. Human cells, on the other hand, have membranes that are composed of relatively neutral phospholipids and cholesterol, which further stabilize the membrane under these conditions. The host cells can therefore survive in the bactericidal environment, which is designed to

https://doi.org/10.1021/acsomega.3c03984
ACS Omega 2023, 8, 36919−36932

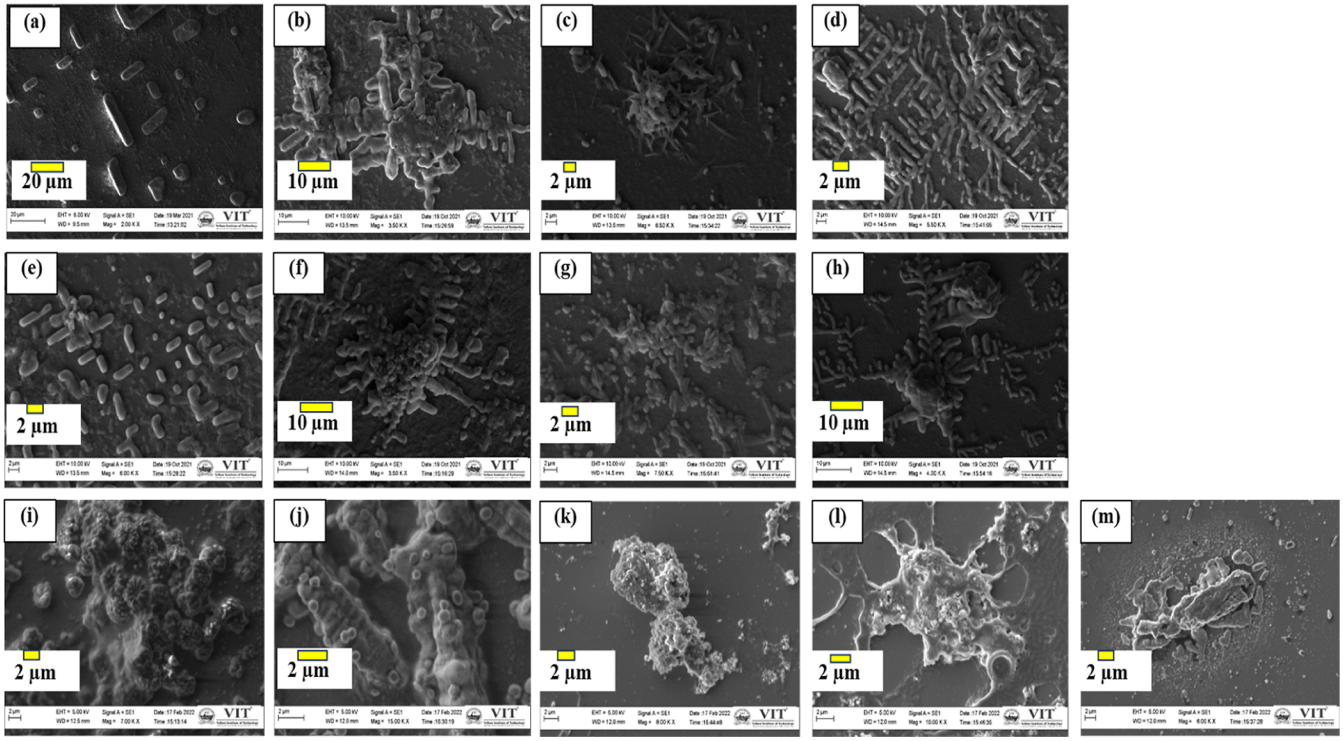

Figure 12. SEM images of (a) *P. aeruginosa* control, (b) ML, (c) MS, (d) MR ceramic powders, (e) *S. epidermidis* control, (f) ML, (g) MS, (h) MR ceramic powders, (i) *A. niger* control, (j) *F. oxysporum* control, (k) ML, (l) MS, and (m) MR ceramic powders.

Table 7. Percentage of Anti-inflammatory HRBC Assay on Different Ceramic Powders

concentration in mg/mL	% inhibition of ceramic powder ML	% inhibition of ceramic powder MS	% inhibition of ceramic powder MR	control drug (diclofenac)
0.5 mg/mL	92.3 ± 0.1%	95.1 ± 0.1%	95.9 ± 0.1%	98.04 ± 0.1%
1 mg/mL	95.1 ± 0.1%	95.7 ± 0.2%	96.1 ± 0.1%	
2 mg/mL	95.9 ± 0.2%	96.15 ± 0.1%	97.54 ± 0.2%	

target only the invading bacteria.[40,51] Oxygen is one of the most essential molecules in the life of all living species. However, the activity of oxygen may be damaging to all living organisms since ionizing radiation and certain reducing agents can damage the cell membranes of bacteria among other things. Furthermore, when active oxygen species such as H_2O_2, O^{2-}, and OH^- were formed, the enzymes and nucleic acids present in bacteria were damaged or destroyed, indicating that the situation was harmful. One of the elements in the antimicrobial mechanism of the monticellite ceramic powders ($CaO-MgO-SiO_2$) is that they form active oxygen species, which is one of the factors in their antibacterial mechanism.[52] To this end, it is worth noting that anaerobic bacteria such as *Bacteroides*, *P. streptococcus*, *Fusobacterium*, and *Clostridium* spp. play a key role in bone infection causing osteomyelitis. Thus, the antibacterial properties of monticellite against anaerobic bacteria will be the topic of future research to tack bone infections.[52,53]

Scanning electron microscopy (SEM) was used to analyze the interaction of monticellite ceramic powder particles with clinical microorganisms (Figure 12). Due to biocompatibility effects, calcium silicate ceramic powders cluster on microorganisms and break the cell membrane protein, resulting in the leaching of proteins and the genetic material.[53] SEM pictures of control plates containing pathogens and treated plates containing ceramic particles are collected. The SEM pictures revealed that monticellite ceramic particles clustered among and around harmful bacteria and fungus strains. When compared to the postexperiment control strain, the pathogenic bacteria *P. aeruginosa* (Figure 12a) and *S. epidermidis* (Figure 12e) were shown to have smooth surfaces coated in aggregates of the particles. In terms of antifungal activity, ceramic powders ML and MR showed more antifungal activity against *Fusarium* sp, whereas MS had greater antifungal activity against *Aspergillus* sp. All the three ceramic powder samples were discovered on the fungal surface and had been broken up into small fragments by the fungal spores. As a result, the impact of the ceramic powders on antibacterial and antifungal activities was validated.

2.6. Anti-inflammatory Analysis. Inflammation is a natural response of the body to an injury or infection. However, when it comes to biomedical applications like implants, excessive or prolonged inflammation can lead to complications and hinder the healing process.[54] Silicate ceramics, as foreign materials, can trigger an inflammatory response in the surrounding tissues. Anti-inflammatory studies evaluate how the presence of silicate ceramics affects the inflammatory response at the implant site. Researchers examine if the material induces an excessive inflammatory reaction or if it helps to mitigate inflammation, promoting better tissue integration and healing.[55] The monticellite ceramic powders provided considerable protection from human red blood cell (HRBC) membrane rupture, which was caused by a hypotonic saline solution in a laboratory

https://doi.org/10.1021/acsomega.3c03984
ACS Omega 2023, 8, 36919−36932

Table 8. Percentage of Hemolysis Assay on Different Ceramic Powders

concentration in mg/mL	% hemolysis of ceramic powder ML	% hemolysis of ceramic powder MS	% hemolysis of ceramic powder MR	positive control drug (diclofenac)	negative control
0.5 mg/mL	1.7 ± 0.1%	3.3 ± 0.2%	1.8 ± 0.1%	0.98 ± 0.1%	0.046 ± 0.1%
1 mg/mL	2.3 ± 0.2%	4.2 ± 0.1%	2.6 ± 0.1%		
2 mg/mL	2.6 ± 0.1%	4.5 ± 0.1%	3.2 ± 0.1%		

setting. The effect may be related to the resistance shown by the ceramic powders in the degradation of the erythrocyte membrane during the treatment. The MR ceramic powder is more effective when compared to the ML and MS ceramic powders, as can be seen Table 7. Diclofenac was utilized as a control medication in this study, and it had an anti-inflammatory activity of 98.04 ± 0.1%.

2.7. Hemolysis Assay. Hemolysis is the process by which the cytoplasmic membrane of red blood cells is lysed, releasing the protein hemoglobin containing oxygen into the blood plasma. It is a characteristic occurrence that happens when foreign objects come into contact with the blood. Thus, hemolysis test is a critical metric for determining the biocompatibility of any synthetic material with blood in order to determine its suitability for usage as an implant material in the body.[56−58] From Table 8, when compared to the control, MS ceramic powder exhibits more hemolytic activity than ML and MR ceramic powders (diclofenac). The hemolysis % increased as the concentration of the ceramic particles increased. MS exhibited a maximum hemolysis rate of 4.5 ± 0.1% at a concentration of 2 mg/mL ceramic powder, which is less than the allowed limit of 5%. Thus, the hemolysis experiment demonstrates that monticellite powder is biocompatible and nonhemolytic.

3. CONCLUSIONS

In the current investigation, monticellite bioceramic was successfully synthesized with an effective sol−gel-assisted combustion technique with different fuel−oxidant ratios. The implementation of varied conditions of metal ion-to-fuel ratios resulted in the formation of a single phasic monticellite at 900 °C. The results of the experiment divulged that the phase formation in attaining the pure phase of monticellite was reduced in comparison to the preceding works of literature with crystallite sizes ranging from 27 to 34 nm. SEM and TEM investigation results concluded that varied fuel ratios produced agglomerated particles with pores over the surface of the material. The in vitro test results unveiled that fuel-lean-originated monticellite showed better apatite deposition on 9 days of immersion in the physiological environment than MS and MR. Alongside, the monticellite nanopowders possessed higher mechanical stability than the previous findings. The novel monticellite bioceramic powder that has been developed has outstanding antibacterial and antifungal inhibitory properties at a lower concentration of 2 mg/mL. It also exhibited the greatest anti-inflammatory percentage and the most favorable prevention of human cell hemolysis, making it suitable for use in bone tissue engineering and a variety of other biomedical applications. The primary results on the material properties and in vitro evaluation satisfied the basic criteria for employing the material for hard tissue engineering. However, the material's in vivo evaluation should be investigated for its real-time utilization.

4. EXPERIMENTAL SECTION

4.1. Synthesis. Combustion-assisted sol−gel technique was utilized for the synthesis of monticellite with different metal ion−fuel ratios. The required amount of calcium nitrate tetrahydrate AR (98%, SD-Fine Chemicals Limited (SDFCL), Mumbai, India), magnesium nitrate hexahydrate AR (98%, SDFCL), tetraethyl orthosilicate (98%, Sigma-Aldrich, Bangalore, India), citric acid AR (99.5%, SDFCL), and concentrated nitric acid AR (98%, SDFCL) was dissolved in double-distilled water. The fuel was mixed in the following ratios: stoichiometric (metal ion/fuel = 1:1), fuel-lean (metal ion/fuel = 1:0.5), and fuel-rich (metal ion/fuel = 1:2). Then, concentrated nitric acid was added dropwise to acclimate the pH of the solution to 1.7 and to form the homogeneous state of the solution, thereby initiating the polycondensation reaction to form a dense gel. The samples were dried in a hot air oven at 100 °C for 2−3 days after dense gel formation. The dried gel was incinerated at 400 °C and calcined at higher temperatures for achieving the pure phase of monticellite.

4.2. Characterization. The analysis of the functional groups in the precursor and calcined samples was conducted using FT-IR analysis with an IR affinity^{-1} Shimadzu FT-IR spectrophotometer (Shimadzu, Japan) from 4000 to 400 cm^{-1}. Under atmospheric conditions, the thermal behavior of the precursor was investigated using thermogravimetric analysis (SDT Q600 V20.9 Build 20, Universal V4.5A TA Instruments, USA) from room temperature to 1200 °C at a heating rate of 10 °C/min. The phase evolution of the samples was investigated using an X-ray diffractometer (Bruker, D8 advance, Germany) with Cu Kα, Ni-filtered radiation. The material's surface framework and energy-dispersive X-ray spectrum were attained using EVO I8 Research (Carl Zeiss, India) at an accelerating voltage of 20 kV. Transmission electron microscopy was used to investigate the particle nature and morphology of the material (FEI-Tecnai G2 20S-TWIN High-resolution, USA).

4.3. In Vitro Bioactivity and Mechanical Studies. The pure monticellite material was weighed, crumbled, and made into cylindrical pellets by employing a pressure of about 5 tonnes with a hydraulic pellet maker with the measurements of 12 mm × 6 mm diameter and thickness as per the ASTM standard, respectively. The pellets were sintered at 900 °C for 2 h. Then, the material was immersed in a physiological medium to investigate the apatite growth ability of the material. The SBF solution which contains the ionic concentration that corresponds to that of the human blood plasma was composed of calcium chloride AR (98%, SDFCL), concentrated hydrochloric acid LR (35−38%, SDFCL), dipotassium hydrogen orthophosphate AR (99%, SDFCL), magnesium chloride AR (99%, SDFCL), potassium chloride AR (99.5%, SDFCL), sodium bicarbonate AR (99%, SDFCL), sodium chloride AR (99%, SDFCL), sodium sulfate anhydrous AR (99.5%, SDFCL), and tris(hydroxymethyl) aminomethane AR (99.8%, SDFCL). The preparation of SBF solution was carried out as per the Kokubo and Takadama method.[59] The

https://doi.org/10.1021/acsomega.3c03984
ACS Omega 2023, 8, 36919−36932

procedure to be carried out for biomineralization and mechanical properties were discussed in our previous reports.[13]

4.4. Antimicrobial Studies. Monticellite was tested for antibacterial and antifungal activities against four clinical pathogens and two fungal cultures. Two from each group, such as Gram-positive organisms (*S. aureus* and *S. epidermidis*) and Gram-negative organisms (*E. coli* and *P. aeruginosa*), were chosen to test their antibacterial activity. *S. aureus* (MTCC 902), *P. aeruginosa* (MTCC 424), *E. coli* (MTCC 46), and *S. epidermidis* were obtained from the Microbial Biotechnology Lab, SBST, VIT. Microbial Biotechnology Laboratory cultures of *A. niger* and *F. oxysporum* were used to test the antifungal activity. The bacterial cultures were revived on plates of nutrient agar medium and incubated at 37 °C for 24 h. A bacterial suspension of 1×10^8 cfu/mL was prepared using a physiological sterile solution. Using a UV spectrophotometer, the optical density of the bacterial culture density was adjusted to 1 O.D.

The antibacterial activity of monticellite powders was tested by using the broth dilution method. Luria−Bertani broth, 100 mL, containing various monticellite concentration levels (0.5, 1, and 2 mg/mL) was added to three different 250 mL Erlenmeyer flasks and with 500 mL of clinical pathogenic organisms. The control flasks were made with LB broth without monticellite powders. For 24 h, the flasks were kept in a rotary shaker at 37 °C. After incubation, the bacterial growth was recorded at 600 nm using an ELISA reader (BioTek-elx800). The inhibition percentage was calculated using the formula shown below (eq 6).[40]

$$\text{Percentage of inhibition (\%)} = \frac{\text{CF} - \text{BCF}}{\text{CF}} \times 100 \quad (6)$$

where CF and BCF denote the control broth with test bacterial strains and final concentration (200 μL) of the monticellite powder with the organism, respectively.

In addition, 100 μL of the control and sample was added to the Muller−Hinton Agar medium for colony formation and bactericidal effect by counting the number of bacterial colonies that appeared on the agar plate. The test was carried out in triplicate, and concordant readings were recorded. In addition to the spread plate method, the agar well diffusion method was also performed to evaluate the antimicrobial activity. A 24 h-old bacterial broth culture was swabbed onto Mueller Hinton agar, and wells were bored on the agar. Monticellite powders at different concentrations of 0.5, 1, and 2 mg were added to the well. Control plates were also kept silicate-free. The Petri plates were incubated for 24 h at 37 °C. The inhibition zone was measured (diameter in mm), and the antibacterial activity of the ceramic powder was also calculated.

The broth dilution technique was employed to determine the antifungal activity of monticellite powders. In different flasks, 100 mL of potato dextrose broth containing various monticellite concentrations of 0.5, 1, and 2 mg/mL were added with 500 μL of clinical pathogens in 250 mL of Erlenmeyer flasks. The control flasks were kept free of monticellite powder, as well. The flasks were incubated in a rotary shaker at 37 °C for 48 h. Following incubation, the samples were filtered through Whatman filter paper, and the dry weight of the fungus was determined. The interaction of the clinical pathogens with the calcium silicate bioceramic (monticellite) powder was analyzed using a scanning electron microscope (Zeiss Evo 18, Smart Sem Software).

4.5. Anti-inflammatory Activity—HRBC Membrane Stabilization Method. The membrane stabilization method was used to test the anti-inflammatory effect on HRBC. For this test, healthy volunteers' blood samples were collected. 5 mL of blood and an equal volume of sterilized Alsever solution (dextrose 2%, sodium citrate 0.8%, citric acid 0.05%, and sodium chloride 0.42% in water) were mixed. The blood sample was centrifuged in isosaline (0.85%) at pH 7 at 3000 rpm. Two packed cells were washed, and a 10% v/v isosaline suspension was prepared. The assay solution contains 0.5 mL of HRBC suspension, 1 mL of phosphate buffer (0.15 M, pH 7.4), 2 mL of hyposaline (0.36%), and monticellite powders of ML, MS, and MR concentrations ranging from 0.5 to 2 mg/mL. For the positive control, diclofenac (Sigma-Aldrich, India) was used, with distilled water as a negative control instead of hyposaline, 2 mL. All samples were centrifuged after 30 min of incubation at 37 °C.[60] A spectrophotometer set to 560 nm was used to estimate the amount of hemoglobin in the supernatant solution. To determine the anti-inflammatory percentage, it was assumed that the amount of hemolysis produced in the presence of distilled water was 100%. The following formula was used to calculate the percentage of hemolysis

$$\text{\% Protection} = \frac{100 - \text{optical density of the drug tested}}{\text{optical density of control}} \times 100 \quad (7)$$

4.6. Hemolysis Assay. A healthy volunteer's blood (5 mL) was collected in a centrifuge tube with EDTA as an anticoagulant. RBCs were separated after centrifugation at 1000 rpm for 5 min and washed with PBS buffer three times. 1 mL of washed blood is diluted with 9 mL of PBS after washing. 250 mL of blood in PBS solution was added to different concentrations of ceramic powder with concentrations varying from 0.5, 1, and 2 mg/mL in 5 mL of water.[61] After 1 h of incubation at 37 °C, the absorbance value of hemoglobin was calculated at 545 nm with a reference wavelength of 630 nm. The hemolytic ratio (HR) is computed as follows

$$\text{HR \%} = \frac{D_t - D_{nc}}{D_{pc} - D_{nc}} \times 100 \quad (8)$$

where D_t, D_{pc}, and D_{nc} denote the absorbance of the ceramic powder, absorbance of the positive control (10 mL of distilled water with 0.2 mL of diluted blood), and absorbance of the negative control (10 mL of PBS with 0.2 mL of diluted blood), respectively. To confirm the reproducibility, the tests were performed in triplicates.

■ ASSOCIATED CONTENT

Supporting Information

The Supporting Information is available free of charge at https://pubs.acs.org/doi/10.1021/acsomega.3c03984.

Petri dish images of the monticellite bioceramics (PDF)

■ AUTHOR INFORMATION

Corresponding Author

Sasikumar Swamiappan − *Department of Chemistry, School of Advanced Sciences, Vellore Institute of Technology, Vellore, Tamil Nadu 632 014, India;* orcid.org/0000-0003-2533-4923; Email: ssasikumar@vit.ac.in

https://doi.org/10.1021/acsomega.3c03984
ACS Omega 2023, 8, 36919−36932

Authors

Naveensubramaniam Vijayakumar − *Department of Chemistry, School of Advanced Sciences, Vellore Institute of Technology, Vellore, Tamil Nadu 632 014, India*

Senthil Kumar Venkatraman − *Department of Chemistry, School of Advanced Sciences, Vellore Institute of Technology, Vellore, Tamil Nadu 632 014, India*

Ravindiran Nandakumar − *Department of Chemistry, School of Advanced Sciences, Vellore Institute of Technology, Vellore, Tamil Nadu 632 014, India*

Raveena Ann Alex − *Microbial Biotechnology Laboratory, School of Biosciences and Technology, Vellore Institute of Technology, Vellore, Tamil Nadu 632014, India*

Jayanthi Abraham − *Microbial Biotechnology Laboratory, School of Biosciences and Technology, Vellore Institute of Technology, Vellore, Tamil Nadu 632014, India*

Hossein Mohammadi − *Institute of Energy Infrastructure (IEI), Universiti Tenaga Nasional, Kajang, Selangor 43000, Malaysia*

Mona Ebadi − *Department of Chemical Sciences, Faculty of Science and Technology, Universiti Kebangsaan Malaysia (UKM), Bangi, Selangor 43600, Malaysia*

Complete contact information is available at: https://pubs.acs.org/10.1021/acsomega.3c03984

Notes

The authors declare no competing financial interest.

■ ACKNOWLEDGMENTS

The authors present their sincere thanks to VIT management for providing necessary help to carry out this research, which was financially supported by the Vellore Institute of Technology Research Grants for Engineering, Management, and Science (VITRGEMS). The authors also thank DST-FIST for XRD analysis, the SEM/EDX facility, and CAMPT-VIT for helping with the mechanical studies.

■ REFERENCES

(1) Vijayakumar, N.; Venkatraman, S. K.; Choudhary, R.; Indurkar, A.; Chatterjee, A.; Abraham, J.; Ostrovskiy, S.; Senatov, F.; Locs, J.; Swamiappan, S. Conversion of Biowaste into Larnite by Sol-Gel Combustion Route for Biomedical Applications. *ChemistrySelect* **2022**, *7*, No. e202103783.

(2) Tian, L.; Tang, N.; Ngai, T.; Wu, C.; Ruan, Y.; Huang, L.; Qin, L. Hybrid fracture fixation systems developed for orthopaedic applications: A general review. *J. Orthop. Translat.* **2019**, *16*, 1−13.

(3) Qin, D.; Wang, N.; You, X. G.; Zhang, A. D.; Chen, X. G.; Liu, Y. Collagen-based biocomposites inspired by bone hierarchical structures for advanced bone regeneration: Ongoing research and perspectives. *Biomater. Sci.* **2022**, *10*, 318−353.

(4) Kim, T.; See, C. W.; Li, X.; Zhu, D. Orthopedic implants and devices for bone fractures and defects: Past, present and perspective. *Eng. Regen.* **2020**, *1*, 6−18.

(5) Fioretta, E. S.; Von Boehmer, L.; Generali, M.; Hoerstrup, S. P.; Emmert, M. Y. Off-the-Shelf Tissue-Engineered Vascular Conduits: Clinical Translation. In *Tissue-Engineered Vascular Grafts*; Walpoth, B. H., Bergmeister, H., Bowlin, G. L., Kong, D., Rotmans, J. I., Zilla, P., Eds.; Springer: Cham, 2020; pp 489−531.

(6) Venkatraman, S. K.; Swamiappan, S. Review on calcium-and magnesium-based silicates for bone tissue engineering applications. *J. Biomed. Mater. Res., Part A* **2020**, *108*, 1546−1562.

(7) Haugen, H. J.; Lyngstadaas, S. P.; Rossi, F.; Perale, G. Bone grafts: which is the ideal biomaterial? *J. Clin. Periodontol.* **2019**, *46*, 92−102.

(8) Turnbull, G.; Clarke, J.; Picard, F.; Riches, P.; Jia, L.; Han, F.; Li, B.; Shu, W. 3D bioactive composite scaffolds for bone tissue engineering. *Bioact. Mater.* **2018**, *3*, 278−314.

(9) Vijayakumar, N.; Bulygina, I.; Lvov, V.; Choudhary, R.; Venkatraman, S. K.; Senatov, F.; Kaloshkin, S.; Swamiappan, S. Effect of Formulation on the Release Kinetics of the Antibiotics from Biocompatible Ceramics. *Trends Biomater. Artif. Organs* **2022**, *36*, 11.

(10) Hutmacher, D. W.; Cool, S. Concepts of scaffold-based tissue engineering—the rationale to use solid free-form fabrication techniques. *J. Cell. Mol. Med.* **2007**, *11*, 654−669.

(11) Lutolf, M. P.; Hubbell, J. A. Synthetic biomaterials as instructive extracellular microenvironments for morphogenesis in tissue engineering. *Nat. Biotechnol.* **2005**, *23* (1), 47−55.

(12) Shekhawat, D.; Singh, A.; Banerjee, M. K.; Singh, T.; Patnaik, A. Bioceramic composites for orthopaedic applications: A comprehensive review of mechanical, biological, and microstructural properties. *Ceram. Int.* **2021**, *47*, 3013−3030.

(13) Collin, M. S.; Venkatraman, S. K.; Sriramulu, M.; Shanmugam, S.; Drweesh, E. A.; Elnagar, M. M.; Mosa, E. S.; Sasikumar, S. Solution combustion synthesis of functional diopside, akermanite, and merwinite bioceramics: Excellent biomineralization, mechanical strength, and antibacterial ability. *Mater. Today Commun.* **2021**, *27*, 102365.

(14) Fernandes, H. R.; Gaddam, A.; Rebelo, A.; Brazete, D.; Stan, G. E.; Ferreira, J. M. Bioactive glasses and glass-ceramics for healthcare applications in bone regeneration and tissue engineering. *Materials* **2018**, *11*, 2530.

(15) Choudhary, R.; Venkatraman, S. K.; Chatterjee, A.; Vecstaudza, J.; Yáñez-Gascón, M. J.; Perez-Sanchez, H.; Locs, J.; Abraham, J.; Swamiappan, S. Biomineralization, antibacterial activity and mechanical properties of biowaste derived diopside nanopowders. *Adv. Power. Technol.* **2019**, *30*, 1950−1964.

(16) Hafezi-Ardakani, M.; Moztarzadeh, F.; Rabiee, M.; Talebi, A. R. Synthesis, and characterization of nanocrystalline merwinite ($Ca_3Mg(SiO_4)_2$) via sol-gel method. *Ceram. Int.* **2011**, *37*, 175−180.

(17) Vijayakumar, N.; Swamiappan, S. Influence of fuels on monticellite synthesis via combustion method. *Mater. Lett.* **2022**, *308*, 131183.

(18) Wu, C.; Chang, J. Degradation, bioactivity, and cytocompatibility of diopside, akermanite, and bredigite ceramics. *J. Biomed. Mater. Res., Part B* **2007**, *83*, 153−160.

(19) Wu, C.; Ramaswamy, Y.; Zreiqat, H. Porous diopside ($CaMgSi_2O_6$) scaffold: A promising bioactive material for bone tissue engineering. *Acta Biomater.* **2010**, *6*, 2237−2245.

(20) Chen, X.; Ou, J.; Wei, Y.; Huang, Z.; Kang, Y.; Yin, G. Effect of MgO contents on the mechanical properties and biological performances of bioceramics in the MgO-CaO-SiO_2 system. *J. Mater. Sci.: Mater. Med.* **2010**, *21*, 1463−1471.

(21) Hench, L. L. Bioceramics: from concept to clinic. *J. Am. Ceram. Soc.* **1991**, *74*, 1487−1510.

(22) Ma, J.; Huang, B. X.; Zhao, X. C.; Ban, C. L.; Hao, X. H.; Wang, C. Z. In vitro degradability and apatite-formation ability of monticellite ($CaMgSiO_4$) bioceramic. *Ceram. Int.* **2019**, *45*, 3754−3759.

(23) Koroglu, L.; Cagirman, G.; Dagaslan, E.; Ayas, E. Microstructural development and in vitro bioactivity of luminescent Eu doped monticellite based ceramics as multifunctional bone graft substitutes. *Mater. Technol.* **2022**, *37*, 422−428.

(24) Venkatraman, S. K.; Choudhary, R.; Krishnamurithy, G.; Balaji Raghavendran, H. R.; Murali, M. R.; Kamarul, T.; Suresh, A.; Abraham, J.; Praharaj, S.; Swamiappan, S. Comparative investigation on antibacterial, biological and mechanical behaviour of monticellite and diopside derived from biowaste for bone regeneration. *Mater. Chem. Phys.* **2022**, *286*, 126157.

(25) Koroglu, L.; Peksen, C. The effect of particle size and phosphorous content in biomineralization media on in vitro bioactivity of monticellite based ceramic powders obtained from boron derivative waste. *Bol. Soc. Esp. Ceram. Vidrio* **2021**, *60*, 93−108.

(26) Chen, X.; Ou, J.; Kang, Y.; Huang, Z.; Zhu, H.; Yin, G.; Wen, H. Synthesis and characteristics of monticellite bioactive ceramic. *J. Mater. Sci.: Mater. Med.* **2008**, *19* (3), 1257−1263.
(27) Barutça, B.; Köroğlu, L.; Ayas, E.; Koparal, A. T. In vitro cytotoxicity of monticellite based bioactive ceramic powder synthesized from boron derivative waste. *Ceram. Int.* **2018**, *44*, 8094−8099.
(28) Venkatraman, S. K.; Swamiappan, S. Synthesis, bioactivity, and mechanical stability of Mg/Ca silicate biocomposites developed for tissue engineering applications. *ChemistrySelect* **2019**, *4*, 13099−13108.
(29) Bakhsheshi-Rad, H. R.; Chen, X. B.; Ismail, A. F.; Aziz, M.; Hamzah, E.; Najafinezhad, A. A new multifunctional monticellite-ciprofloxacin scaffold: preparation, bioactivity, biocompatibility, and antibacterial properties. *Mater. Chem. Phys.* **2019**, *222*, 118−131.
(30) Koppala, S.; D Souza, R. M.; Sivanandam, P.; Tammina, S. K.; Xu, L.; Li, K.; Chen, Q.; Balan, R.; Devarepally, K. K.; Swamiappan, S. Sol gel combustion derived monticellite bioceramic powders for apatite formation ability evaluation. *Mater. Res. Exp.* **2020**, *6*, 125431.
(31) Kalantari, E.; Naghib, S. M.; Reza Naimi-Jamal, M.; Mozafari, M. Green solvent-based sol-gel synthesis of monticellite nanoparticles: a rapid and efficient approach. *J. Sol-Gel Sci. Technol.* **2017**, *84*, 87−95.
(32) Koroglu, L.; Ayas, E. A systematic study on solid-state synthesis of monticellite ($CaMgSiO_4$) based ceramic powders obtained from boron derivative waste. *Adv. Powder Technol.* **2018**, *29*, 2835−2844.
(33) Esposito, S. Traditional" sol-gel chemistry as a powerful tool for the preparation of supported metal and metal oxide catalysts. *Materials* **2019**, *12*, 668.
(34) Sasikumar, S.; Vijayaraghavan, R. Solution combustion synthesis of bioceramic calcium phosphates by single and mixed fuels - a comparative study. *Ceram. Int.* **2008**, *34*, 1373−1379.
(35) Boobalan, K.; Varun, A.; Vijayaraghavan, R.; Chidambaram, K.; Mudali, U. K. Facile, scalable synthesis of nanocrystalline calcium zirconate by the solution combustion method. *Ceram. Int.* **2014**, *40*, 5781−5786.
(36) Boobalan, K.; Vijayaraghavan, R.; Chidambaram, K.; Mudali, U. M. K.; Raj, B. Preparation, and characterization of nanocrystalline zirconia powders by the glowing combustion method. *J. Am. Ceram. Soc.* **2010**, *93*, 3651−3656.
(37) Saberi, A.; Negahdari, Z.; Alinejad, B.; Golestani-Fard, F. Synthesis and characterization of nanocrystalline forsterite through citrate-nitrate route. *Ceram. Int.* **2009**, *35*, 1705−1708.
(38) Iwata, N. Y.; Lee, G. H.; Tokuoka, Y.; Kawashima, N. Sintering behavior and apatite formation of diopside prepared by coprecipitation process. *Colloids Surf., B* **2004**, *34*, 239−245.
(39) Kazemi, A.; Abdellahi, M.; Khajeh-Sharafabadi, A.; Khandan, A.; Ozada, N. Study of in vitro bioactivity and mechanical properties of diopside nano-bioceramic synthesized by a facile method using eggshell as raw material. *Mater. Sci. Eng., C* **2017**, *71*, 604−610.
(40) Venkatraman, S. K.; Choudhary, R.; Krishnamurithy, G.; Raghavendran, H. R. B.; Murali, M. R.; Kamarul, T.; Suresh, A.; Abraham, J.; Swamiappan, S. Biomineralization, mechanical, anti-bacterial and biological investigation of larnite and rankinite bioceramics. *Mater. Sci. Eng., C* **2021**, *118*, 111466.
(41) Moroni, L.; Licht, R.; de Boer, J.; de Wijn, J. R.; van Blitterswijk, C. A. Fiber diameter and texture of electrospun PEOT/PBT scaffolds influence human mesenchymal stem cell proliferation and morphology, and the release of incorporated compounds. *Biomaterials* **2006**, *27*, 4911−4922.
(42) Wang, W.; Yeung, K. W. Bone grafts and biomaterials substitutes for bone defect repair: A review. *Bioact. Mater.* **2017**, *2*, 224−247.
(43) Kalantari, E.; Naghib, S. M. A comparative study on biological properties of novel nanostructured monticellite-based composites with hydroxyapatite bioceramic. *Mater. Sci. Eng., C* **2019**, *98*, 1087−1096.
(44) Kalantari, E.; Naghib, S. M.; Naimi-Jamal, M. R.; Esmaeili, R.; Majidzadeh-A, K.; Mozafari, M. Nanostructured monticellite: an emerging player in tissue engineering. *Mater. Today: Proc.* **2018**, *5*, 15744−15753.
(45) Li, J. J.; Kaplan, D. L.; Zreiqat, H. Scaffold-based regeneration of skeletal tissues to meet clinical challenges. *J. Mater. Chem. B* **2014**, *2*, 7272−7306.
(46) Rh Owen, G.; Dard, M.; Larjava, H. Hydoxyapatite/beta-tricalcium phosphate biphasic ceramics as regenerative material for the repair of complex bone defects: BIPHASIC CERAMICS AS REGENERATIVE MATERIAL IN BONE DEFECTS. *J. Biomed. Mater. Res., Part B* **2018**, *106*, 2493−2512.
(47) Shamoradi, F.; Emadi, R.; Ghomi, H. Fabrication of monticellite-akermanite nanocomposite powder for tissue engineering applications. *J. Alloys Compd.* **2017**, *693*, 601−605.
(48) Gerhardt, L. C.; Boccaccini, A. R. Bioactive glass and glass-ceramic scaffolds for bone tissue engineering. *Materials* **2010**, *3*, 3867−3910.
(49) Campoccia, D.; Montanaro, L.; Arciola, C. R. The significance of infection related to orthopedic devices and issues of antibiotic resistance. *Biomaterials* **2006**, *27*, 2331−2339.
(50) Fu, J. X.; Wang, H. J.; Zhou, Y. Q.; Wang, J. Y. Antibacterial activity of ciprofloxacin-loaded zein microsphere films. *Mater. Sci. Eng., C* **2009**, *29*, 1161−1166.
(51) Škrlová, K.; Malachová, K.; Muñoz-Bonilla, A.; Měřinská, D.; Rybková, Z.; Fernández-García, M.; Plachá, D. Biocompatible polymer materials with antimicrobial properties for preparation of stents. *Nanomaterials* **2019**, *9*, 1548.
(52) Sawai, J.; Kawada, E.; Kanou, F.; Igarashi, H.; Hashimoto, A.; Kokugan, T.; Shimizu, M. Detection of active oxygen generated from ceramic powders having antibacterial activity. *J. Chem. Eng. Jpn.* **1996**, *29*, 627−633.
(53) Li, Q.; Mahendra, S.; Lyon, D. Y.; Brunet, L.; Liga, M. V.; Li, D.; Alvarez, P. J. Antimicrobial nanomaterials for water disinfection and microbial control: potential applications and implications. *Water Res.* **2008**, *42*, 4591−4602.
(54) Saha, S.; Lestari, W.; Dini, C.; Sarian, M. N.; Hermawan, H.; Barao, V. A.; Sukotjo, C.; Takoudis, C. Corrosion in Mg-alloy biomedical implants-the strategies to reduce the impact of the corrosion inflammatory reaction and microbial activity. *J. Magnesium Alloys* **2022**, *10*, 3306−3326.
(55) Zhu, Y.; Shen, Y.; Xiang, Y.; Fang, K.; Xu, K.; Ma, P.; Cai, C.; Ma, J.; Shen, X. Combined application of silica particles and zirconium hydrogen phosphate coating to improve the friction resistance and osteogenic/anti-inflammatory properties of micro-arc oxidation-treated titanium. *Surf. Coat. Technol.* **2022**, *451*, 129037.
(56) Majumdar, S.; Hira, S. K.; Tripathi, H.; Kumar, A. S.; Manna, P. P.; Singh, S. P.; Krishnamurthy, S. Synthesis and characterization of barium-doped bioactive glass with potential anti-inflammatory activity. *Ceram. Int.* **2021**, *47*, 7143−7158.
(57) Rathinam, K.; Sivakumar, R.; Saraswati, V. In vivo and in vitro evaluation of a bio machinable glass ceramic. *Bull. Mater. Sci.* **1994**, *17*, 171−179.
(58) Seyfert, U. T.; Biehl, V.; Schenk, J. In vitro hemocompatibility testing of biomaterials according to the ISO 10993−4. *Biomol. Eng.* **2002**, *19*, 91−96.
(59) Kokubo, T.; Takadama, H. How useful is SBF in predicting in vivo bone bioactivity? *Biomaterials* **2006**, *27*, 2907−2915.
(60) Dhanalakshmi, C. P.; Vijayalakshmi, L.; Narayanan, V. Synthesis, and preliminary characterization of polyethylene glycol (PEG)/hydroxyapatite (HAp) nanocomposite for biomedical applications. *Int. J. Phys. Sci.* **2012**, *7*, 2093−2101.
(61) Tsamesidis, I.; Kazeli, K.; Pouroutzidou, G.; Reybier, K.; Pantaleo, A.; Lymperaki, E.; Kontonasaki, E. Evaluation of hemolytic activity and oxidative stress biomarkers in erythrocytes after exposure to bioactive glass nanoceramics. *Beilstein* **2019**, *1*, 201985.

https://doi.org/10.1021/acsomega.3c03984
ACS Omega 2023, 8, 36919−36932